OPEN

Light: Science & Applications (2014) 3, e209; doi:10.1038/lsa.2014.90

www.nature.com/lsa

ORIGINAL ARTICLE

320-fold luminescence enhancement of $[Ru(dpp)_3]Cl_2$ dispersed on PMMA opal photonic crystals and highly improved oxygen sensing performance

Pingwei Zhou[1], Donglei Zhou[1], Li Tao[1], Yongsheng Zhu[1,2], Wen Xu[1], Sai Xu[1], Shaobo Cui[1,2], Lin Xu[1] and Hongwei Song[1]

Ru complexes ($[Ru(dpp)_3]Cl_2$) were spin coated on poly(methyl methacrylate) (PMMA) opal photonic crystals (PhCs), and a ~320-fold luminescence enhancement was observed compared to that on glass, which is the largest luminescence enhancement of dye molecules by the modulation of three-dimensional (3D) PhCs reported until now. The enhancement mechanism was carefully examined and it was shown that the luminescence of $[Ru(dpp)_3]Cl_2$ depended on the molecule concentration and temperature. It can be concluded that the suppressed non-radiative relaxation among the molecules and the field enhancement both contribute significantly to the luminescence enhancement. The PMMA PhC/Ru complex composites were then tested for their intracellular oxygen sensing and cell imaging properties; these composites effectively improved the limit of detection (LOD) and the brightness of the cell images.
Light: Science & Applications (2014) **3,** e209; doi:10.1038/lsa.2014.90; published online 10 October 2014

Keywords: cell imaging; fluorescence enhancement; oxygen sensing; photonic crystals

INTRODUCTION

Luminescence sensing and imaging is currently one of the most widely used techniques for environmental monitoring, disease diagnosis and genomic/proteomic research.[1] In most cases, the practical application requires that the luminescence sensing is performed with a weaker pumping light; therefore, luminescence enhancement has profound significance for obtaining higher sensitivity and a lower limit of detection (LOD). Until now, various methods have been explored to enhance the luminescence intensity during luminescence sensing, including optical fiber sensing, surface-plasmon-induced luminescence enhancement and the modulation of photonic crystals (PhCs).[2–4] Among the various techniques related to luminescence enhancement, the modulation of PhCs has attracted considerable interest and has yielded a wide variety of applications.[5–13] PhCs can largely enhance the luminescence of dyes/quantum dots, and through theoretical simulation, the excitation field can be largely enhanced.[14,15] In particular, not only can three-dimensional (3D) opal or inverse opal PhCs largely enhance the luminescence of dyes but they also have the advantage of easier preparation. As reported by Song's group,[16,17] a 40-fold enhancement in luminescence was observed using 3D PhCs for optical storage, and a 162-fold enhancement was obtained by modulating dual stopband PhCs. As reported by Li's group,[18] a 71-fold enhancement was also observed using 3D PhCs. In most of these cases, luminescence enhancement was attributed to the excitation field enhancement effect. Although the excitation field can be enhanced by 3D PhCs through theoretical simulation,[19] the practical process of luminescence enhancement is more complex, and the essential mechanism should be further discussed to obtain more significant enhancement.

In this work, a ~320-fold enhancement was observed based on the coupling of $[Ru(dpp)_3]Cl_2$ with 3D poly(methyl methacrylate) (PMMA) opal PhCs, which is the largest enhancement using 3D PhCs until now. The enhancement mechanism was determined based on the emissions of $[Ru(dpp)_3]Cl_2$ on dye concentration dispersed on the PMMA PhCs and temperature. The PMMA PhC/Ru complex composites were also used for assistant intracellular oxygen sensing and cell imaging, which effectively improved the LOD and the brightness of the cell images.

MATERIALS AND METHODS

Preparation of PMMA PhCs

The PMMA spheres were synthesized following the steps below.[20] First, methyl methacrylate (MMA) was washed with NaOH solution (0.01 g mL^{-1}) to remove the polymerization inhibitor.[21] Second, 3-mL MMA solution and 40-mL deionized water were placed into a three-necked bottle. Polymerization was performed by oil bath heating at 90 ℃ for 1.5 h with magnetic stirring and 18-mg of potassium persulfate as an initiator. Finally, the milk white solution with suspended PMMA spheres was obtained. By changing the amount of MMA solution in the above recipe, the diameter of PMMA spheres could be perfectly tuned. By varying the MMA solution amount from 2.7-mL to 3.4-mL in 0.1-mL steps, spheres of different sizes were obtained.

[1]State Key Laboratory on Integrated Optoelectronics, College of Electronic Science and Engineering, Jilin University, Changchun 130012, China and [2]College of Physics, Jilin University, Changchun 130012, China
Correspondence: Professor HW Song, College of Electronic Science and Engineering, Jilin University, 2699 Qianjin Street, Changchun 130012, China
E-mail: songhw@jlu.edu.cn
Received 18 April 2014; revised 21 July 2014; accepted 22 July 2014

PMMA PhCs were synthesized through the vertical deposition method by growing the PMMA spheres onto the glass substrate.[22] First, 60-mL deionized water and 3-mL of the precursor solution were prepared before being placed into a 100-mL plastic beaker. Second, a hydrophilic glass substrate was vertically inserted into the plastic beaker. The solution was naturally evaporated in a drying oven at 32 ℃ for 24 h, and the PMMA spheres self-assembled on the glass substrate through hydrophilic interactions. Finally, the PhCs were placed into the drying oven at 120 ℃ for 40 min to improve their physical stability. Additionally, the stopband of the PhCs was finely controlled *via* the diameter of the PMMA spheres, which ranged from 390 to 625 nm in diameter.

Luminescence measurement

The $[Ru(dpp)_3]Cl_2$ (Sigma-Aldrich Corporation, Saint Louis, MO, USA) was dissolved in ethanol solution with a concentration of 0.4 mg mL^{-1}. Then, 6-μL of the solution was spin-coated onto the PhCs and the glass (1500 r.p.m., 20 s). The spectra of $[Ru(dpp)_3]Cl_2$ were measured using a confocal laser scanning microscope with an excitation light at 455 nm.

Cytotoxicity

The cytotoxicity of the PMMA PhCs was determined by the following experiments. Human breast cancer cells (MCF-7, suspended) were cultured in Dulbecco's modified Eagle's medium supplemented with 10% fetal bovine serum at 37 ℃ in a 5%-CO_2 incubator. PMMA PhCs on the glass substrate (2 cm^2 $piece^{-1}$) were preplaced at the bottom of a 12-well plate through ultraviolet irradiation. Then, 1-mL of an MCF-7 cell suspension (1.6×10^5 cells mL^{-1}) was seeded per well and exposed to PMMA PhCs, and the cells were incubated for additional periods ranging from 2 to 24 h. Untreated cells were used as a control (100% viability). At the end of the exposure, 20-mL of the cell suspension was removed and mixed with the same volume of 0.4%-trypan-blue solution. Following cell staining for 2 min, an aliquot (10 μL) of the stained cell suspension was pipetted onto a hemocytometer and counted for the cell number. Finally, the obtained cell viability was expressed relative to the control.

Oxygen sensing of the MCF-7 cells

$[Ru(dpp)_3]Cl_2$ at a concentration of 20 μg mL^{-1} was incubated together with MCF-7 cells in chamber slides at 37 ℃ for 12 h under 5%-CO_2 gas. The glass with PMMA PhCs and pure glass were placed into the confocal dish. Then, 0.05-mL of the MCF-7 cell suspension was added to the PMMA PhC and glass surfaces. Gas with different oxygen concentrations was piped into the confocal dish, and a sealing film was used to create an independent environment. The MCF-7 cells were viewed *in vitro* with a confocal laser scanning microscope under continuous pumping of a 455-nm laser.

RESULTS AND DISCUSSION

Structural features

PhCs possess spatial periodicity in their dielectric constants on the length scale of the optical wavelength. Consequently, PhCs respond to electromagnetic waves in a similar way to how atomic crystals respond to electrons. Because an electronic band gap is created by the periodic arrangement of atoms in a semiconductor, the periodic electromagnetic modulation created by the PhCs can yield a PSB (photonic stopband), a band of frequency for which light propagation in the PhCs is forbidden. The PhCs prepared with different sizes of PMMA spheres can exhibit different spatial periodicities in their dielectric constants and yield different PSBs. Figure 1a shows the transmission spectra of the PhCs with different stopbands, and the inset of Figure 1a shows the relationship between the PSB and the diameter of PMMA spheres. The PSB positions were well described by the Bragg diffraction[23] equation using the PMMA sphere diameters measured by SEM (scanning electron microscope). Figure 1b and 1c shows the SEM image and side-view image of a PhC with a PSB at 455 nm. The PMMA spheres yielded a long-ranged ordered structure,

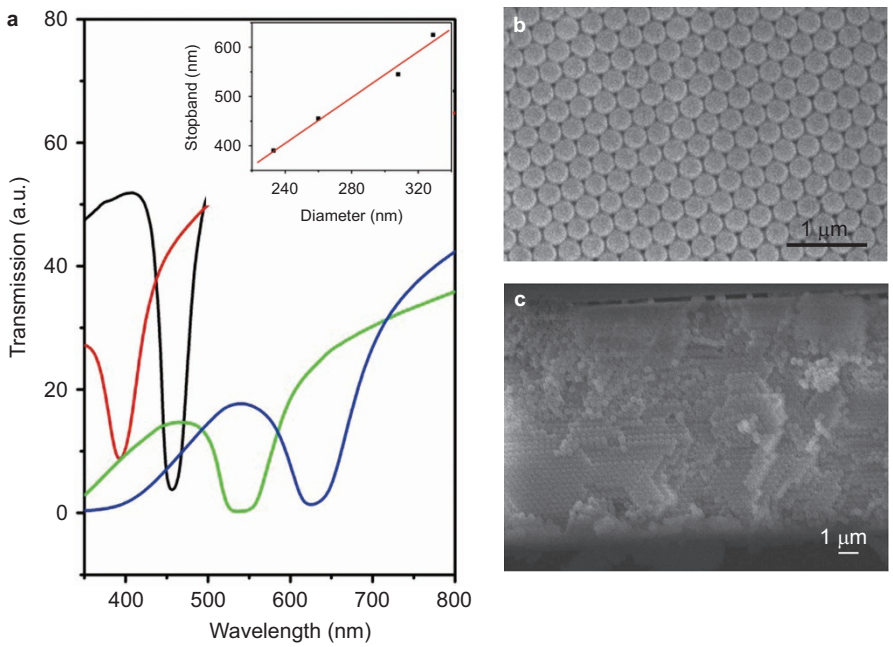

Figure 1 (**a**) Transmission spectra of the PhCs with different stopbands. Inset: the relationship between the PSB and the PMMA sphere diameter. (**b**) SEM image of a PhC with a PSB at 455 nm. (**c**) Side-view image of a PhC with a PSB at 455 nm. PhC, photonic crystal; PMMA, poly(methyl methacrylate); PSB, photonic stopband; SEM, scanning electron microscope.

doi:10.1038/lsa.2014.90

suggesting the formation of well-organized PhCs. As presented in Figure 1c, the PhC thickness was approximately 10 μm, and the PhC structure was composed of approximately 40 layers of PMMA spheres.

The relative amount of $[Ru(dpp)_3]Cl_2$ molecules on the PhC/glass samples

To ensure the same density of the $[Ru(dpp)_3]Cl_2$ molecules on the PhC and the glass, the same 6-μL solution of $[Ru(dpp)_3]Cl_2$ molecules (0.4 mg mL^{-1}) was taken and spin-coated onto the PhC and the glass. Because the amount of solution was small and the rotation speed of the spin coater was slower, after spin-coating, the thin film of $[Ru(dpp)_3]Cl_2$ molecules was distributed within a circle area, and no solution was spin-coated outside the samples. The areas of the PhC sample and the glass sample were determined to be 1.33 cm^2 and 1.54 cm^2, respectively. To verify the homogeneity of the two samples, five points were randomly chosen from the circles (Supplementary Fig. S1) of the two samples, and the luminescence intensity of each point was measured. The luminescence intensity rarely changed, indicating that the $[Ru(dpp)_3]Cl_2$ molecules were distributed uniformly. The areas of the circles on the PhC and the glass were nearly the same, indicating that the number of $[Ru(dpp)_3]Cl_2$ molecules at each point was similar. To further determine the number of $[Ru(dpp)_3]Cl_2$ molecules, the absorption spectra of $[Ru(dpp)_3]Cl_2$ on the glass and on the PhCs were measured and compared, as shown in Figure 2. The red line shows the absorption spectrum of the PhC with a PSB at 410 nm, and the black line shows the absorption spectrum of the same PhC coated with $[Ru(dpp)_3]Cl_2$ molecules. To distinguish the absorption coefficient of $[Ru(dpp)_3]Cl_2$, the PSB of the PhC was chosen far from the absorption of $[Ru(dpp)_3]Cl_2$. The absorption of the PhC ranging from 450 to 500 nm improved after being coating with $[Ru(dpp)_3]Cl_2$ molecules, which suggests that the $[Ru(dpp)_3]Cl_2$ molecules successfully adhered to the PhC surface. The absorption coefficient of $[Ru(dpp)_3]Cl_2$ on the PhC was determined by subtracting the red line from the black line and is presented in the Figure 2 inset (red dots). The black dots display the absorption spectrum of $[Ru(dpp)_3]Cl_2$ on glass. As indicated in the Figure 2 inset, the absorption strength of $[Ru(dpp)_3]Cl_2$ on the PhC was very close to that on the glass, indicating that the number of $[Ru(dpp)_3]Cl_2$ molecules on the PhC was nearly identical to that on the glass.

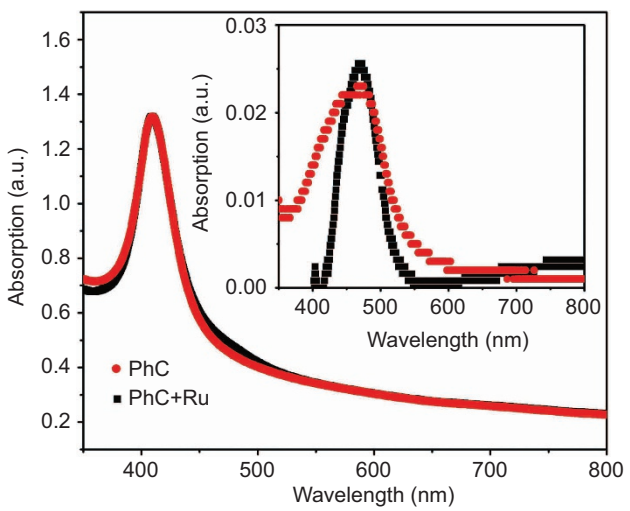

Figure 2 Absorption spectra of the blank PhC (red) and the PhC coated with $[Ru(dpp)_3]Cl_2$ (black). Inset: a comparison of the absorption spectra of $[Ru(dpp)_3]Cl_2$ coated on the glass (black) and on the PhC (red). PhC, photonic crystal.

Notably, in the present PMMA PhC/$[Ru(dpp)_3]Cl_2$ composites, the distribution of $[Ru(dpp)_3]Cl_2$ molecules in the PMMA PhCs was not homogeneous. To determine the distribution of the molecules, the depth-dependent luminescence intensity was measured using confocal laser scanning microscopy (Supplementary Fig. S2). It can be concluded that the molecule density gradually decreased with the depth of the PMMA PhCs. This suggests that most of the dye molecules distributed on the PMMA PhC surface.

320-fold luminescence enhancement and its mechanism

The emission spectra of $[Ru(dpp)_3]Cl_2$ on the PhC and on the glass were measured by confocal laser scanning microscopy under an excitation light at 455 nm. As shown in Figure 3a, the luminescence intensity of $[Ru(dpp)_3]Cl_2$ coated on the PMMA PhCs was much stronger than that coated on the glass; even the luminescence of $[Ru(dpp)_3]Cl_2$ was enhanced 100 times. The luminescence enhancement factor, which is defined as the ratio of the luminescence intensity of $[Ru(dpp)_3]Cl_2$ coated on the PMMA PhCs to that on the glass, was determined to be as high as ~320-fold. The inset of Figure 3a displays the digital photograph of the empty glass (right), $[Ru(dpp)_3]Cl_2$ coated on the glass (middle) and $[Ru(dpp)_3]Cl_2$ coated on the PhC (left) under xenon lamp exposure, which further indicates the highly improved red emissions of $[Ru(dpp)_3]Cl_2$ on the PhC.

To reveal the mechanism of luminescent enhancement, the original solution was diluted with absolute ethyl alcohol with different concentrations. Figure 3b and 3c shows the dependence of the enhancement factor and decay time constant on the concentration of $[Ru(dpp)_3]Cl_2$ molecules. Interestingly, the enhancement factor increased gradually with the increased concentration from more than 100 times to 320 times. Notably, when the concentration was lower than 30 μg mL^{-1}, the change was rapid and when the concentration was higher than this value, the change was not obvious. The decay time constant of $[Ru(dpp)_3]Cl_2$ on the glass rapidly decreased with the increased $[Ru(dpp)_3]Cl_2$ concentration, ranging from 8 to 30 μg mL^{-1} and nearly reserved as a constant as the concentration increased further. The decrease in the decay time constant on the molecule concentration was attributed to the energy transfer (ET) among the different molecules. When the molecule concentration was lower, the molecules distributed freely on the glass, and the ET among different molecules was difficult. As the molecule concentration increased, the ET among different molecules increased due to the decreased average distance of the nearby molecules, and the decay time constant decreased with the increased molecule concentration. As the concentration of molecules was high enough, the molecules on the glass were clustered together, and the ET among different molecules was the same, leading to the steady decay time constants. By contrast, the decay time constant of $[Ru(dpp)_3]Cl_2$ on the PhC was approximately 4.1 μs and rarely changed with the concentration, indicating that the PhC structure efficiently restrained the ET among different molecules. Owing to the huge surface area, the PhC could effectively disperse the $[Ru(dpp)_3]Cl_2$ molecules, preventing the ET among the dye molecules. Additionally, the decay time constant of $[Ru(dpp)_3]Cl_2$ on the PhC increased to approximately 2–4 times that on the glass, depending on the concentration of $[Ru(dpp)_3]Cl_2$. This finding may be mainly attributed to modulation of the effective refractive index on the radiative decay rate and the existence of a solid skeleton on the non-radiative relaxation rate of $[Ru(dpp)_3]Cl_2$ on the PhC. In most of the previous publications related to quantum dots or dye molecules

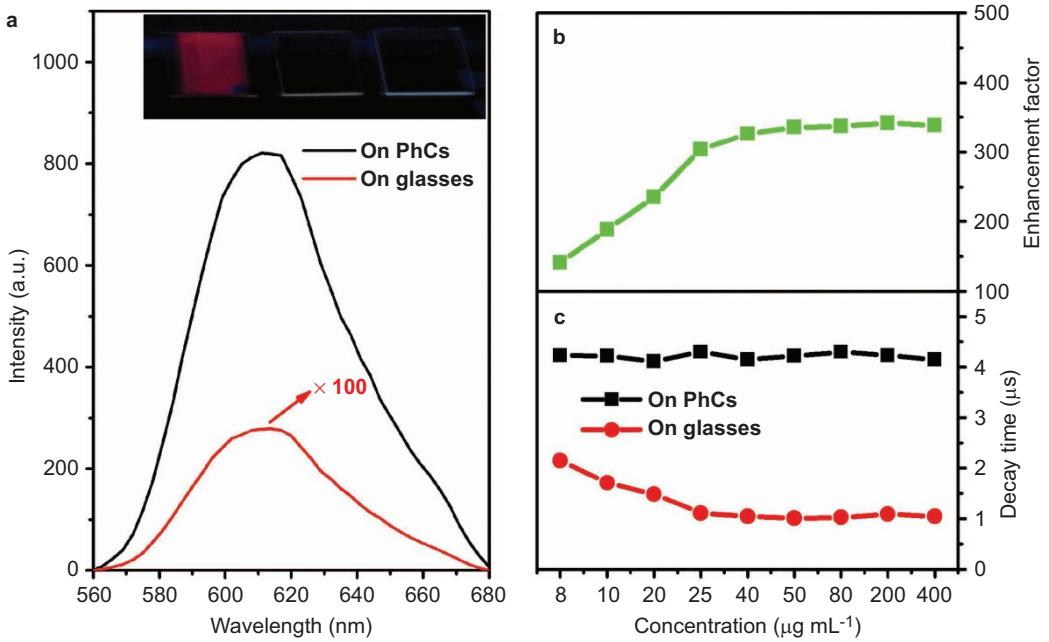

Figure 3 (**a**) Spectra of $[Ru(dpp)_3]Cl_2$ on the PhC (black) and on the glass (red). Inset: digital photograph of $[Ru(dpp)_3]Cl_2$ on the PhC (left), $[Ru(dpp)_3]Cl_2$ on the glass (middle), and the glass (right). (**b**) The enhancement factor. (**c**) Decay time of $[Ru(dpp)_3]Cl_2$ on the PhC (black) and on the glass (red), with different concentrations. PhC, photonic crystal.

inserted into 3D PhCs, an obvious change in the decay time constant was observed.[7,8]

To verify the universality of the PMMA PhC modulation of the dye molecules, the luminescence enhancements for different dyes dispersed on the PMMA PhCs were studied and are presented in Figure 4. When the molecule concentration was fixed at 0.1 mg mL^{-1}, an 84-fold luminescent enhancement was observed for FITC, whereas a 230-fold enhancement was observed for R6G. It was also obvious that for the same dye, the enhancement factor at a higher concentration (0.1 mg mL^{-1}) was much higher compared with that at a lower concentration (2 μg mL^{-1}). Because the surface area of the PhC is much larger than that of the glass, the molecules can be well dispersed and the ET between dye molecules can be largely restrained. The enhancement of excitation field should not vary significantly when different dye molecules are coated on the PhCs when measured at the same conditions. However, a different enhancement factor was obtained for different dye molecules. This finding demonstrates that the luminescence enhancement was obtained for various dye molecules and that the enhancement factor depended on not only the enhanced excitation field, but also the type of dye molecules. This result may be attributed to the changed vibration bonds, the varied ET rate and the variant polarity of the dye molecules. Indeed, as the polarity of the dye molecules changes, the dye–molecule interaction with the PhC skeleton would also change, which would most likely influence the luminescent quantum yield.

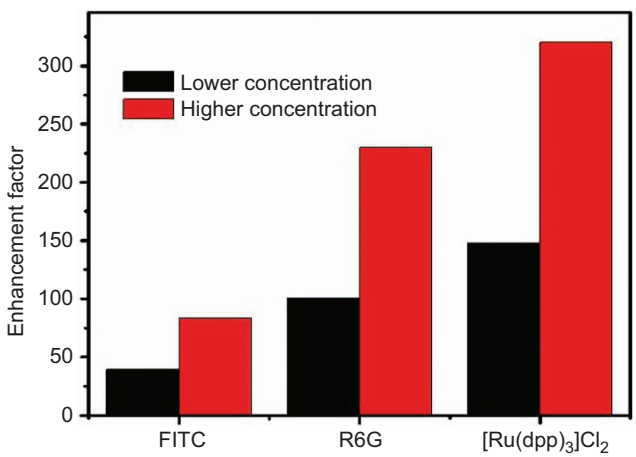

Figure 4 The enhancement factor of FITC, R6G and $[Ru(dpp)_3]Cl_2$ at a lower/higher concentration.

Notably, the highly enhanced luminescence of the dye molecules can be obtained not only by the modulation of 3D PhCs, but also by the scattering of some particles. Previously, some scattering particles, such as TiO_2,[24] were added to sensor films to make the excitation light hit more emitters and the emission light scatter back to the detector.[25] This is also an effective strategy to improve the excitation of the oxygen-sensitive probe and enhance the signals.

To verify the PhC effect, the PhC samples with different PSBs (390, 455, 550 and 625 nm) and a film sample without a PSB (comprising PMMA spheres with different sizes) were prepared. Figure 5a shows the spectra of $[Ru(dpp_3)]Cl_2$ on different samples, and Figure 5b shows the luminescent enhancement factor of different samples. The luminescence intensity of $[Ru(dpp_3)]Cl_2$ on the glass was relatively low, and with different structures composed of PMMA spheres, the luminescence intensity of $[Ru(dpp_3)]Cl_2$ was enhanced at different levels. When using the film without PSB or the PhCs with a PSB far from the excitation light (455 nm), the enhancement factor varied from 120 to 164 (Figure 5, right). In these situations, the excitation light was scattered by PMMA spheres and hit more $[Ru(dpp_3)]Cl_2$ molecules. When using the PhC with a PSB right coupled with the excitation light, the enhancement factor was improved to 320-fold

doi:10.1038/lsa.2014.90

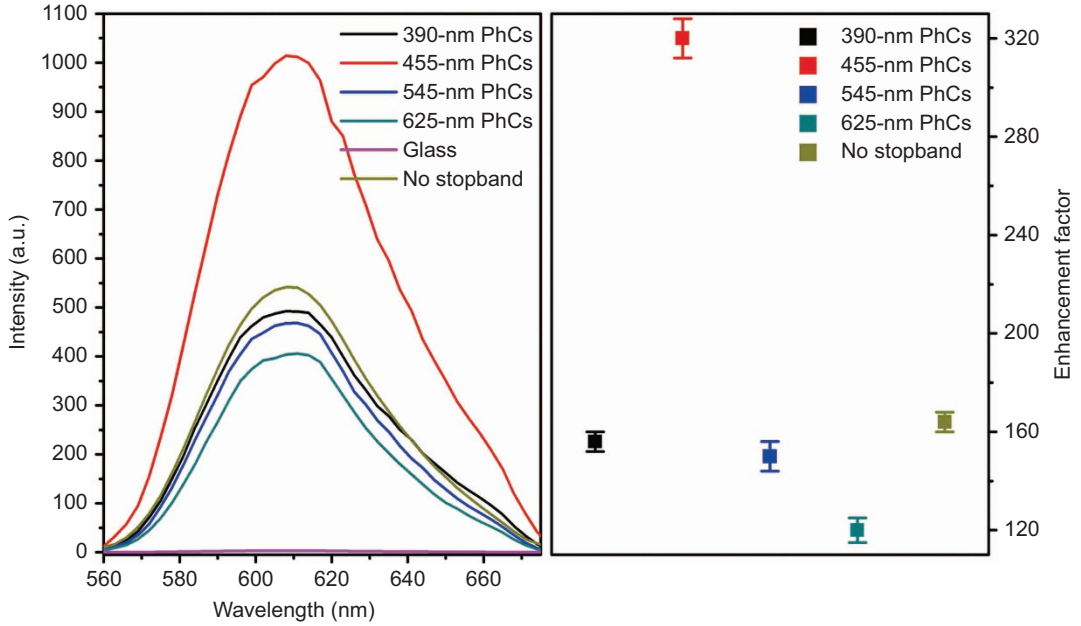

Figure 5 The spectra (left) and enhancement factor (right) of $[Ru(dpp)_3]Cl_2$ on PhCs with different stopbands and on the PMMA film without a stopband were compared to that on glass. PhC, photonic crystal; PMMA, poly(methyl methacrylate).

(Figure 5, right). In this situation, the excitation light coupled with the PhC structure and the scattering was further improved due to the modulation through the periodic dielectric constant. This shows that the existence of a PSB leads to an extra luminescence enhancement of ~2 times. We stimulated the integrated electric field distribution on the depth of the PMMA PhCs by the FDTD (finite difference time domain) method, and the result showed that on the surface of the PhC, the integrated electric field improved by approximately two times in comparison with the position without PSB modulation (Supplementary Fig. S3). As mentioned above, in the recent sample, most of the dye molecules distributed on the surface of the PMMA crystals; therefore, the experimental luminescence enhancement is in accordance with the theoretical stimulation.

Temperature-dependent luminescence and dynamics

Temperature-dependent luminescence and dynamics is critical for determining the radiative and non-radiative transition processes. Figure 6a shows the total luminescence intensity of $[Ru(dpp)_3]Cl_2$

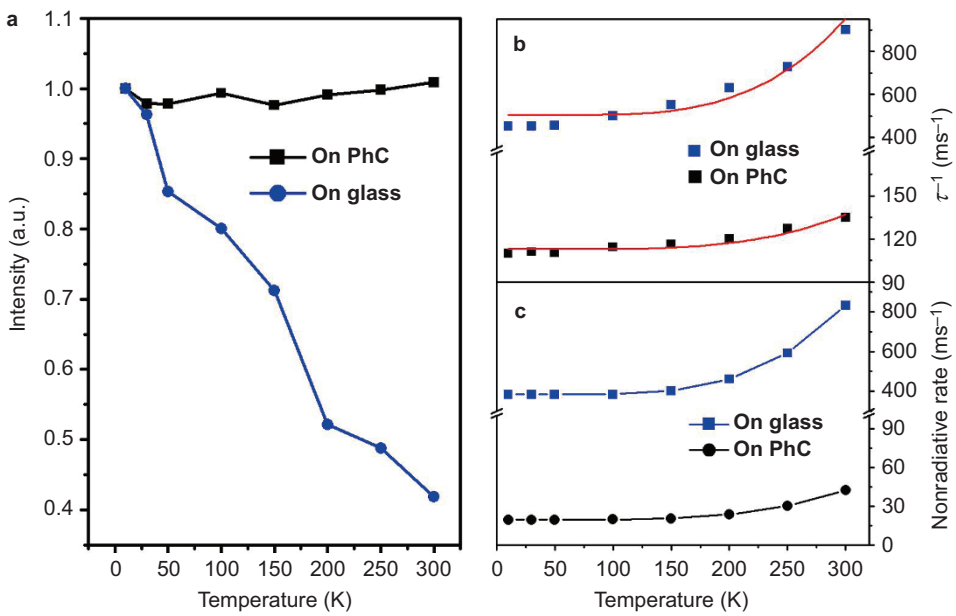

Figure 6 Luminescence intensity (**a**), reciprocal of the decay time and the fitting line (red) (**b**) and the non-radiative rate of $[Ru(dpp)_3]Cl_2$ on PhC (black) and $[Ru(dpp)_3]Cl_2$ on glass (blue) (**c**) with different temperatures. PhC, photonic crystal.

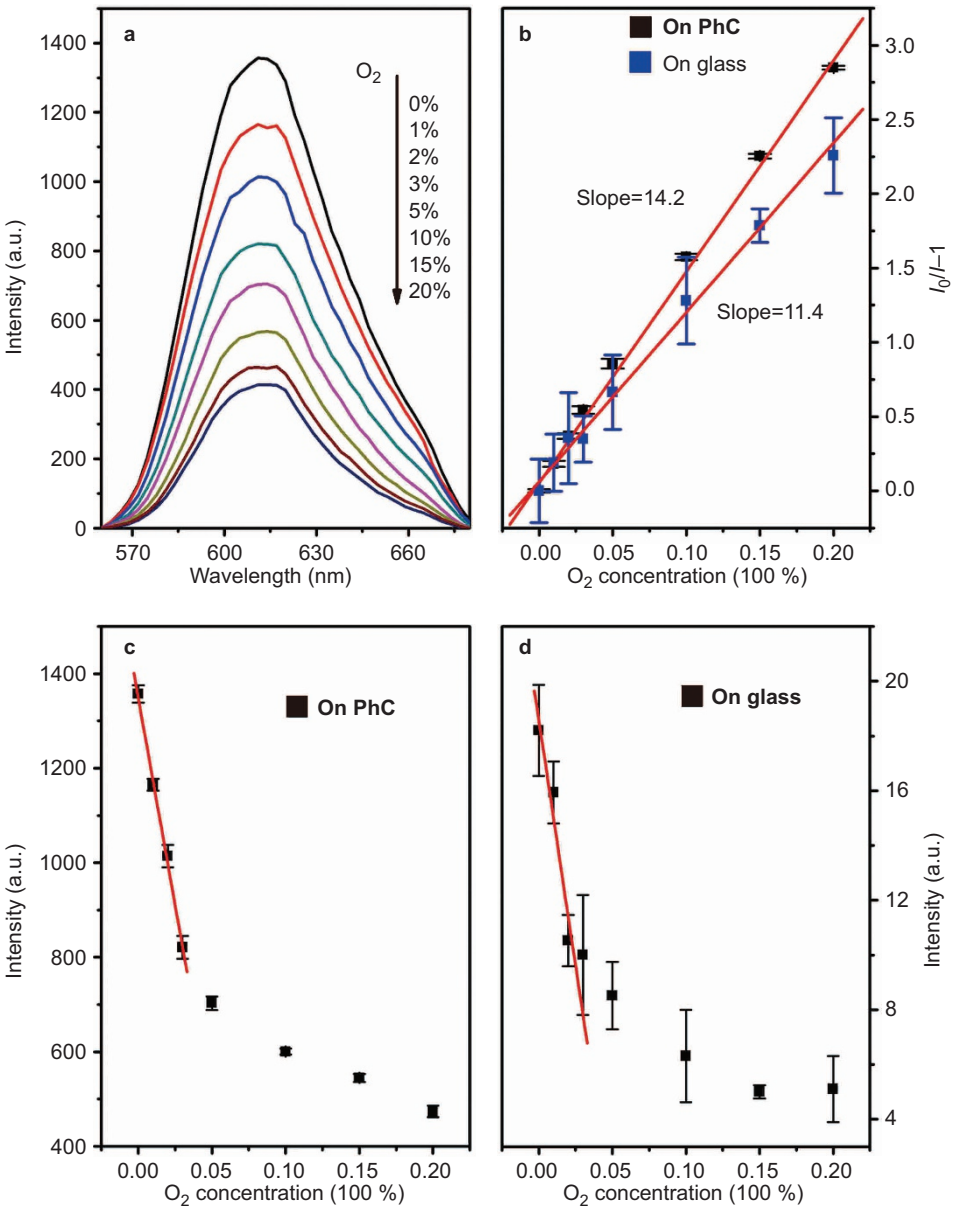

Figure 7 (**a**) Emission spectra of $[Ru(dpp)_3]Cl_2$ on the PhC with different oxygen concentrations. (**b**) ($I_0/I-1$) of $[Ru(dpp)_3]Cl_2$ on the PhC (black dots), glass (blue dots) and fitting line (red line). (**c**, **d**) Luminescence intensity of $[Ru(dpp)_3]Cl_2$ with different oxygen concentrations on the PhC and on the glass. PhC, photonic crystal.

on the PhC and on the glass as a function of temperature under 455-nm excitation. It is obvious that the luminescence intensity of $[Ru(dpp)_3]Cl_2$ on the glass decreased rapidly with the increased temperature, but on the PhC, the luminescence intensity rarely changed with the temperature. This indicates that the temperature quenching of $[Ru(dpp)_3]Cl_2$ can be suppressed considerably on the PhC. As is well established, the non-radiative transition of dye molecules stems from molecule vibration, which increases quickly with elevated temperature, inducing temperature quenching of the luminescence. Because the dye molecules were dispersed into the gaps of the PMMA PhCs, the molecule vibration could be effectively limited due to the framework of the PMMA solid. To further determine the radiative and non-radiative relaxation rates in different samples, the temperature dependence of the reverse of the decay time constant of $[Ru(dpp)_3]Cl_2$ on the PhC and on the glass are presented in Figure 6b. As is well known, the non-radiative relaxation rate improves greatly with increased temperature due to highly improved molecule vibration. Compared with the non-radiative relaxation rate, the change of radiative transition rate for the emitters is not obvious. Based on the multi-phonon-relaxation theory, the total $[Ru(dpp)_3]Cl_2$ decay rate (the reverse of the decay time, designated as W_{Total}) can be written as follows:[26]

$$W_{Total} = W_R + W_{NR}(0)\left(1 - e^{-\hbar\omega/kT}\right)^{-\Delta E/\hbar\omega} \quad (1)$$

where W_R is the radiative transition rate and $W_{NR}(0)$ is the non-radiative relaxation rate at 0 K. Through the calculation, W_R was determined to be 122.35 ms^{-1} on the glass and 92.3 ms^{-1} on the PhC. $W_{NR}(0)$ was determined to be 383.7 ms^{-1} on the glass and

doi:10.1038/lsa.2014.90

20.6 ms^{-1} on the PhC. According to the theory of the virtual-cavity model, the radiative transition rate can be written as follows:[27]

$$W_R \approx f(ED)\frac{\left[\frac{1}{3}\left(n_{eff}^2+2\right)\right]^2 n_{eff}}{\lambda_0^2} \quad (2)$$

where f(ED) is the electric dipole strength and n_{eff} is the effective refractive index of the medium. The n_{eff} of the PhC sample and the glass sample are 1.15 and 1.27, respectively. Through Equation (2), W_R on the glass is approximately 1.38 times that on the PhC, which is in accordance with the experimental data. It is obvious that the $W_{NR}(0)$ of $[Ru(dpp)_3]Cl_2$ was restrained largely with the assistance of PMMA PhC in contrast with that on the glass, and the dependence of the non-radiative rate of $[Ru(dpp)_3]Cl_2$ on temperature was calculated by Equation (1) and is presented in Figure 6c.

Using the W_R and W_{NR} values calculated above, the internal quantum efficiency of $[Ru(dpp)_3]Cl_2$ on the PhC (η_{PhC}) and on the glass (η_{glass}) as a function of temperature was determined. At room temperature, η_{PhC}=68.6% and η_{glass}=12.8%. It is surprising that the internal quantum efficiency improves 5.36-fold due to largely restrained non-radiative relaxation. Because of the introduction of the PhC solid skeleton, the non-radiative relaxation can be largely restrained[28,29] and a similar phenomenon was also observed in rare earth ions inserted in inverse opal PhCs.[30] Additionally, the influence of photobleaching was also considered and can be ignored due to the short measurement time (Supplementary Fig. S4).

Overall, a 320-fold enhancement was observed based on the coupling of $[Ru(dpp)_3]Cl_2$ with 3D PMMA PhCs. In addition to the excitation field modulation, the suppression of ET between $[Ru(dpp)_3]Cl_2$ and non-radiative transition of the dye molecules dispersed on the PMMC PhCs also played an important role in the luminescence enhancement.

Highly improved oxygen sensing properties

Based on this 320-fold enhancement, the gaseous oxygen sensing, intracellular oxygen sensing and cell imaging properties of $[Ru(dpp)_3]Cl_2$ were studied with the assistance of PMMA opal PhCs. In traditional gaseous oxygen sensing, the luminescence spectra of the dye with different oxygen concentrations are displayed in Figure 7a. According to the spectra, the luminescence intensity of $[Ru(dpp)_3]Cl_2$ on PhC gradually decreased with the increased oxygen concentration. This oxygen optical sensing scheme is based on the quenching of $[Ru(dpp)_3]Cl_2$ by molecular oxygen, so the luminescence intensity can be described by the Stern–Volmer expression.

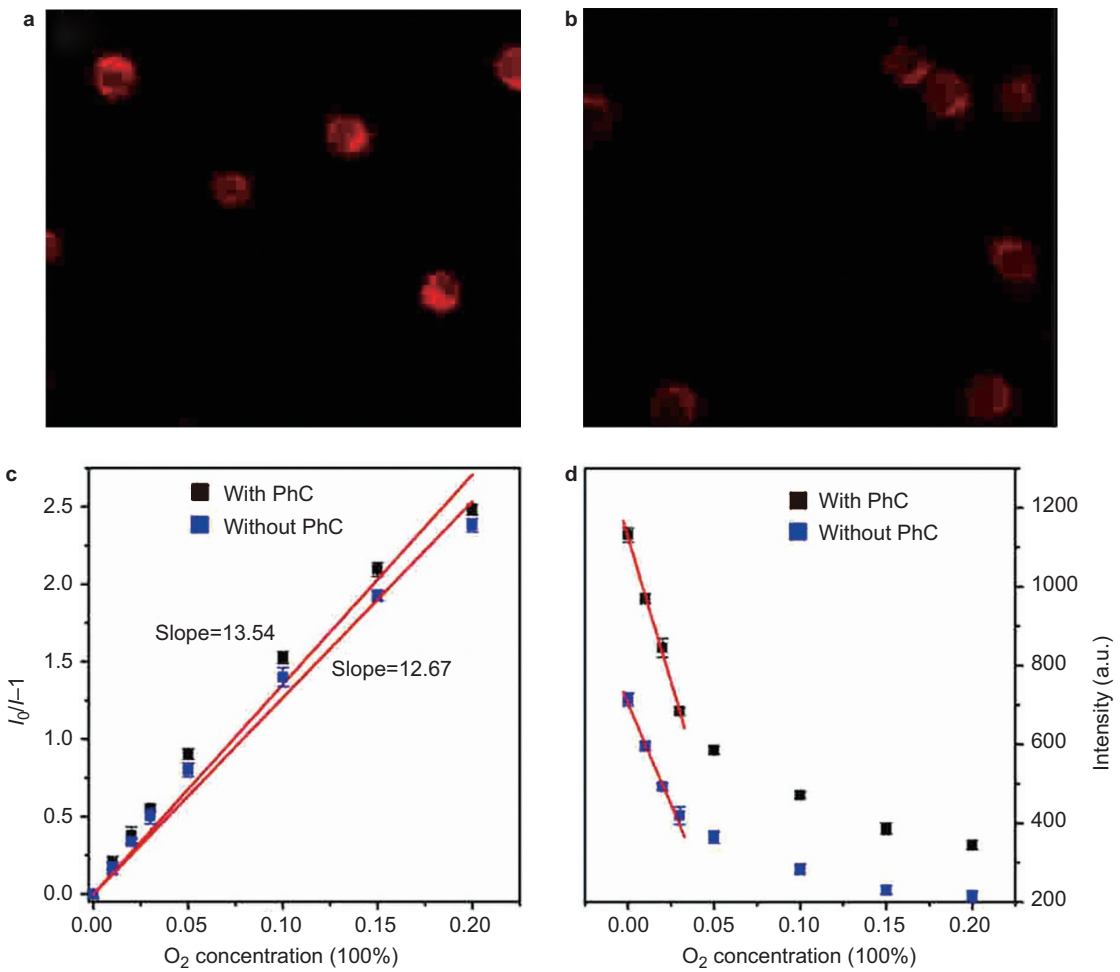

Figure 8 Confocal image of the MCF-7 cells on the PhC (**a**) and on the glass (**b**), respectively. (**c**) ($I_0/I-1$) of $[Ru(dpp)_3]Cl_2$ on the PhC (black dots), glass (blue dots) and fitting line (red line). (**d**) The luminescence intensity of $[Ru(dpp)_3]Cl_2$ in MCF-7 cells with different oxygen concentrations on the PhC (black dots) and on the glass (blue dots), respectively. PhC, photonic crystal.

Figure 7b shows the highly linear relationship between $(I_0/I-1)$ and the oxygen concentration. The sensitivity (I_0/I_{20}) was determined to be 3.8 for the PhC sample and 3.3 for the glass sample. The non-radiative relaxation can be largely restrained due to the introduction of PhC solid skeleton, and more electrons in the triplet excitation state can be quenched by oxygen, so the sensitivity of the PhC sample is higher than that of glass sample. It should be highlighted that compared with the other study on oxygen sensing using $Ru(dpp)_3$, the sensitivity of the PhC sample is not outstanding, but the quantum efficiency of the PhC sample is the highest one (68.6%). According to Wang's review,[25] at a low oxygen concentration, the signal change is maximal and almost linear. Figure 6c and 6d shows the luminescence intensity of $[Ru(dpp)_3]Cl_2$ on the PhC and on the glass, respectively and it was almost linear when the oxygen concentration ranged from 0% to 3%. Through the calculation, the LOD (3S/N: S, standard deviation; N, slope)[31] for oxygen on the PhC and on the glass are 5 ppm and 497 ppm, respectively. Interestingly, the samples of the $[Ru(dpp)_3]Cl_2$ on the PhC demonstrate a much lower LOD of oxygen than that on the glass.

Figure 8a and 8b displays the luminescence images of MCF-7 cells in air with and without the assistance of PMMA PhC, respectively. It is obvious that with the assistance of PMMA PhC, the luminescence image of MCF-7 cells became more distinct and bright compared with those without the assistance of PMMA PhC. Because the $[Ru(dpp)_3]Cl_2$ molecules are dispersed in the cytoplasm and the size of MCF-7 cells is approximately several microns, $[Ru(dpp)_3]Cl_2$ and PMMA PhC have far-field interactions. In this situation, PMMA PhC acted as a reflect substrate and only a 1.7-fold enhancement was obtained. Figure 8c shows the highly linear relationship between $(I_0/I-1)$ and the oxygen concentration. The sensitivity (I_0/I_{20}) was determined to be 3.4 for the PhC sample and 3.5 for the glass sample. The sensitivity was almost the same because the interaction between the oxygen and $[Ru(dpp)_3]Cl_2$ molecules was similar (both in the cytoplasm). Figure 8d displays the luminescence intensity of $[Ru(dpp)_3]Cl_2$ in MCF-7 cells with different oxygen concentrations on the PhC (black dots) and on the glass (blue dots), respectively. Through the calculation, the LOD for oxygen in MCF-7 cells is 6 ppm with the assistance of PhC, which is lower than that without the assistance of PhC (11 ppm). In addition, the cytotoxicity test was conducted to verify the biocompatibility of the PMMA PhCs. Figure 9 shows the cell viability of PMMA PhCs on MCF-7 cells at various hours. It is evident that the cell viability is over 90% after 24 h, indicating that the toxicity of the PMMA PhCs is minimal.

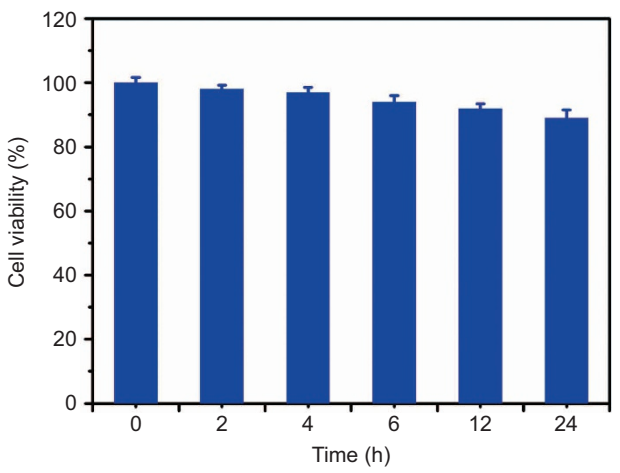

Figure 9 Cell viability of PMMA PhCs on MCF-7 cells at different hours. PMMA, poly(methyl methacrylate). PhC, photonic crystal.

In a study[32] using polystyrene nanoparticles loaded with modified $Ru(dpp)_3$ as optical oxygen sensing probe, the sensing and imaging of intracellular oxygen following two-photon excitation were successfully achieved. The background absorption and luminescence of the biomatter became weaker through near-infrared excitation. In the present work, we focused more on employing the PhC structure for oxygen sensing and imaging. Using unmodified $[Ru(dpp)_3]Cl_2$ as the probe, through the assistance of PhC structure, a 1.7-fold enhancement was achieved for the cell imaging brightness, and intracellular oxygen sensing at an oxygen concentration from 0% to 20% was obtained. Additionally, the LOD was improved through the assistance of the PhC structure.

CONCLUSIONS

In summary, a 320-fold enhancement was observed as $[Ru(dpp)_3]Cl_2$ was spin-coated onto PMMA PhCs, which is the largest enhancement using 3D PhCs until now. Its origin was mainly attributed to the suppression of ET between $[Ru(dpp)_3]Cl_2$ molecules and non-radiative transition and the enhancement of the excitation field. The PMMA PhCs/Ru composites were also used for traditional gas sensing, facilitated intracellular oxygen sensing and cell imaging, which exhibited a highly improved performance.

ACKNOWLEDGEMENTS

This work was supported by the Major State Basic Research Development Program of China (No. 2014CB643506), the National Natural Science Foundation of China (Grant Nos. 11374127, 11304118, 61204015, 81201738, 61177042 and 11174111), the Program for Chang Jiang Scholars and Innovative Research Teams in the University (No. IRT13018).

1 Lakowicz JR. Radiative decay engineering: biophysical and biomedical applications. *Anal Biochem* 2001; **298**: 1–24.
2 Shevchenko Y, Camci-Unal G, Cuttica DF, Dokmeci MR, Albert J *et al*. Surface plasmon resonance fiber sensor for real-time and label-free monitoring of cellular behavior. *Biosens Bioelectron* 2014; **56**: 359–367.
3 Wang HS, Wang C, He YK, Xiao FN, Bao WJ *et al*. Core–shell Ag@SiO_2 nanoparticles concentrated on a micro/nanofluidic device for surface plasmon resonance-enhanced fluorescent detection of highly reactive oxygen species. *Anal Chem* 2014; **86**: 3013–3019.
4 Fenzl C, Hirsch T, Wolfbeis OS. Photonic crystals for chemical sensing and biosensing. *Angew Chem Int Ed* 2014; **53**: 3318–3335.
5 Majumdar A, Kim J, Vuckovic J, Wang F. Electrical control of silicon photonic crystal cavity by graphene. *Nano Lett* 2013; **13**: 515–518.
6 Raineri F, Karle TJ, Roppo V, Monnier P, Raj R. Time-domain mapping of nonlinear pulse propagation in photonic-crystal slow-light waveguides. *Phys Rev A* 2013; **87**: 041802(R).
7 Lodahl P, van Driel AF, Nikolaev IS, Irman A, Overgaag K *et al*. Controlling the dynamics of spontaneous emission from quantum dots by photonic crystals. *Nature* 2004; **430**: 654–657.
8 Ródenas A, Zhou G, Jaque D, Gu M. Rare-earth spontaneous emission control in three-dimensional lithium niobate photonic crystals. *Adv Mater* 2009; **21**: 3526–3530.
9 Kim HJ, Kim S, Jeon H, Ma J, Choi SH *et al*. Fluorescence amplification using colloidal photonic crystal platform in sensing dye-labeled deoxyribonucleic acids. *Sensor Actuat B Chem* 2007; **124**: 147–152.
10 Hu J, Zhao XW, Zhao YJ, Li J, Xu WY *et al*. Photonic crystal hydrogel beads used for multiplex biomolecular detection. *J Mater Chem* 2009; **19**: 5730–5736.
11 Li MZ, He F, Liao Q, Liu J, Xu L *et al*. Ultrasensitive DNA detection using photonic crystals. *Angew Chem Int Ed* 2008; **47**: 7258–7262.
12 Pal S, Fauchet PM, Miller BL. 1-D and 2-D photonic crystals as optical methods for amplifying biomolecular recognition. *Anal Chem* 2012; **84**: 8900–8908.
13 Pokhriyal A, Lu M, Chaudhery V, Huang CS, Schulz S *et al*. Photonic crystal enhanced fluorescence using a quartz substrate to reduce limits of detection. *Opt Express* 2010; **18**: 24793–24808.
14 Ganesh N, Zhang W, Mathias PC, Chow E, Soares JA *et al*. Enhanced fluorescence emission from quantum dots on a photonic crystal surface. *Nat Nanotechnol* 2007; **2**: 515–520.

doi:10.1038/lsa.2014.90

15 Mathias PC, Wu HY, Cunningham BT. Employing two distinct photonic crystal resonances to improve fluorescence enhancement. *Appl Phys Lett* 2009; **95**: 021111.
16 Li H, Wang JX, Lin H, Xu L, Xu W *et al*. Amplification of fluorescent contrast by photonic crystals in optical storage. *Adv Mater* 2010; **22**: 1237–1241.
17 Li H, Wang JX, Liu F, Song YL, Wang RM. Fluorescence enhancement by heterostructure colloidal photonic crystals with dual stopbands. *J Colloid Interface Sci* 2011; **356**: 63–68.
18 Tao CA, Zhu W, An Q, Yang HW, Li WN *et al*. Coupling of nanoparticle plasmons with colloidal photonic crystals as a new strategy to efficiently enhance fluorescence. *J Phys Chem C* 2011; **115**: 20053–20060.
19 Li MZ, Liao Q, Liu Y, Li ZY, Wang JX *et al*. A white-lighting LED system with a highly efficient thin luminous film. *Appl Phys A* 2010; **98**: 85–90.
20 Holland BT, Blanford CF, Do T, Stein A. Synthesis of highly ordered, three-dimensional, macroporous structures of amorphous or crystalline inorganic oxides, phosphates, and hybrid composites. *Chem Mater* 1999; **11**: 795–805.
21 Jiang P, Bertone JF, Hwang KS, Colvin VL. Single-crystal colloidal multilayers of controlled thickness. *Chem Mater* 1999; **11**: 2132–2140.
22 Wang W, Song HW, Bai X, Liu Q, Zhu YS. Modified spontaneous emissions of europium complex in weak PMMA opals. *Phys Chem Chem Phys* 2011; **13**: 18023–18030.
23 Hiltner PA, Krieger IM. Diffraction of light by ordered suspensions. *J Phys Chem* 1969; **73**: 2386–2389.
24 Chojnacki P, Mistlberger G, Klimant I. Separable magnetic sensors for the optical determination of oxygen. *Angew Chem Int Ed* 2007; **46**: 8850–8853.
25 Wang XD, Wolfbeis OS. Optical methods for sensing and imaging oxygen: materials, spectroscopies and applications. *Chem Soc Rev* 2014; **43**: 3666–3761.
26 Song HW, Wang JW, Chen BJ, Peng HS, Lu SZ. Size-dependent electronic transition rates in cubic nanocrystalline europium doped yttria. *Chem Phys Lett* 2003; **376**: 1–5.
27 Peng HS, Song HW, Chen BJ, Wang JW, Lu SZ *et al*. Temperature dependence of luminescent spectra and dynamics in nanocrystalline Y_2O_3:Eu^{3+}. *J Chem Phys* 2003; **118**: 3277–3282.
28 Zhang H, Song HW, Yu HQ, Li SW, Bai X *et al*. Modified photoluminescence properties of rare-earth complex/polymer composite fibers prepared by electrospinning. *Appl Phys Lett* 2007; **90**: 103103.
29 Li Q, Li T, Wu JG. Luminescence of europium(III) and terbium(III) complexes incorporated in poly(vinyl pyrrolidone) matrix. *J Phys Chem B* 2001; **105**: 12293–12296.
30 Zhu YS, Xu W, Zhang HZ, Xu S, Wang YF *et al*. Inhibited local thermal effect in upconversion luminescence of YVO_4:Yb^{3+}, Er^{3+} inverse opals. *Opt Express* 2012; **20**: 29673–29678.
31 Sun Y, Liu Y, Guo W. Fluorescent and chromogenic probes bearing salicylaldehyde hydrazone functionality for cyanide detection in aqueous solution. *Sens Actuators B* 2009; **143**: 171–176.
32 Wang XD, Achatz DE, Hupf C, Sperber M, Wegener J *et al*. Imaging of cellular oxygen *via* two-photon excitation of fluorescent sensor nanoparticles. *Sens Actuators B* 2013; **188**: 257–262.

Supplementary information for this article can be found on the *Light: Science & Applications*' website (http://www.nature.com/lsa/).